HHS Public Access

Author manuscript

Biomater Biosyst. Author manuscript; available in PMC 2022 March 21.

Published in final edited form as:

Biomater Biosyst. 2021 September ; 3: . doi:10.1016/j.bbiosy.2021.100020.

Endothelial barrier function is co-regulated at vessel bifurcations by fluid forces and sphingosine-1-phosphate

Ehsan Akbari[a,‡], **Griffin B. Spychalski**[b,‡], **Miles M. Menyhert**[c], **Kaushik K. Rangharajan**[a], **Joseph W. Tinapple**[b], **Shaurya Prakash**[a,d], **Jonathan W. Song**[a,d,*]

[a]Department of Mechanical and Aerospace Engineering, The Ohio State University, Columbus, OH, United States, 43210

[b]Department of Biomedical Engineering The Ohio State University, Columbus, OH, United States, 43210

[c]Department of Chemical and Biomolecular Engineering, The Ohio State University, Columbus, OH, United States, 43210

[d]Comprehensive Cancer Center, The Ohio State University, Columbus, OH, United States, 43210

Abstract

Sphingosine-1-phosphate (S1P) is a bioactive sphingolipid mediator of endothelial barrier function. Prior studies have implicated mechanical stimulation due to intravascular laminar shear stress in co-regulating S1P signaling in endothelial cells (ECs). Yet, vascular networks in vivo consist of vessel bifurcations, and this geometry generates hemodynamic forces at the bifurcation point distinct from laminar shear stress. However, the role of these forces at vessel bifurcations in regulating S1P-dependent endothelial barrier function is not known. In this study, we implemented a microfluidic platform that recapitulates the flow dynamics of vessel bifurcations with in situ quantification of the permeability of microvessel analogues. Co-application of S1P with impinging bifurcated fluid flow, which is characterized by approximately zero shear stress and 38 dyn•cm^{-2} stagnation pressure at the vessel bifurcation point, promotes vessel stabilization. Similarly, co-treatment of S1P with 3 dyn•cm^{-2} laminar shear stress is also protective of endothelial barrier function. Moreover, it is shown that vessel stabilization due to bifurcated fluid flow and laminar shear stress is dependent on S1P receptor 1 or 2 signaling. Collectively, these findings demonstrate the endothelium-protective function of fluid forces at vessel bifurcations and their involvement in coordinating S1P-dependent regulation of vessel permeability.

Keywords

Vessel permeability; Microfluidic biomimicry; Branched microvessels; Mechanotransduction

*Corresponding author. song.1069@osu.edu (J.W. Song).

‡These authors contributed equally.

Declaration of Competing Interest

The authors declare no conflict of interest.

Supplementary materials

Supplementary material associated with this article can be found, in the online version, at doi:10.1016/j.bbiosy.2021.100020.

1. Introduction

The endothelial cells (ECs) of small blood vessels, such as capillaries and post-capillary venules, form a semi-permeable barrier that control solute transport across the vessel wall [1]. Maintenance of endothelial barrier integrity and permeability is crucial for regulating immune cell trafficking and tissue homeostasis [2, 3]. Accordingly, vascular barrier dysfunction underlies the pathogenesis of inflammation [4], atherosclerosis [5], cancer [6], and other diseases [7]. Furthermore, heightened vessel permeability is a hallmark of pathological angiogenesis [8]. Therefore, a fundamental understanding of the factors that help modulate endothelial barrier integrity is of great importance for restoring normal vascular function during disease conditions.

Sphingosine-1-phosphate (S1P) is a small bioactive lysosphingolipid that signals through its family of G-protein coupled receptors [9]. ECs are known to express three of the five known S1P receptors (S1PR1–3) [10], and S1P exerts pleiotropic effects on EC proliferation, chemo-taxis, and angiogenesis [11–13]. S1P resides primarily in blood plasma at concentrations of 100–1000 nM [14] and is an important regulator of endothelial barrier function [10, 15–17]. Under normal physiological conditions, S1P associates primarily with two protein carriers or chaperones in order to be transported effectively through the bloodstream: high density lipoproteins (HDL; ~65%) and albumin (~35%) [18, 19]. Carrier-bound S1P biases the activation of S1PR1 [20], which is known to enhance endothelial barrier integrity [21, 22]. In contrast, activation of S1PR2 destabilizes endothelial junctions [23]. Unlike carrier-bound S1P, carrier-free S1P engages S1PR1, S1PR2 and S1PR3 with comparable affinity [24]. Correspondingly, elevated levels of carrier-free S1P have been shown to induce a pro-inflammatory and atherogenic phenotype that is concomitant with compromised endothelial barrier function [25–27]. Moreover, S1P production is upregulated in several human cancers compared with normal tissue [28], and antagonizing S1P signaling with targeted therapies [29] has demonstrated anti-angiogenic effects in tumors [30].

In addition to biomolecular signaling, fluid mechanical cues such as laminar shear stress (LSS) that arises in straight regions of the vasculature, are known to be key regulators of vessel function [31–33]. Interestingly, LSS has been shown to upregulate endothelial S1PR1 expression levels [34–36] and induce ligand-independent activation of S1PR1 that leads to suppression of sprouting angiogenesis and vessel stabilization in vivo [36]. Despite these findings, the role of hemodynamic forces in regulating the effects of carrier-free S1P on vessel function, especially in blood vessels that may be affected by fluid forces other than LSS, is poorly understood. Furthermore, while LSS predominantly arises in straight blood vessel segments, it is important to note that vascular networks are hierarchical branching structures that generate stagnation pressure with nearly no shear stress at vessel bifurcations causing mechanical stimulation that is distinct from LSS. [37].

Three dimensional (3-D) microfluidic models of vascular function have been widely implemented for studying vascular biology and physiology under well-defined physical and chemical conditions in vitro [38–41]. However, these models, including ones that studied the effects of S1P [12, 42], feature either a single or two parallel linear channels lined

with ECs [43]. Consequently, to our knowledge, the coordinated responses of carrier-free S1P-signaling and flow dynamics arising at vessel bifurcations in modulating endothelial barrier function has not been investigated. Here, we implemented our previously reported biomimetic microfluidic platform [44, 45] that uniquely combines in vivo settings (i.e., the flow dynamics at vessel bifurcations) with in situ quantification of the endothelial hydraulic conductivity (L_p) of microvessel analogues [44]. We report that under static (i.e., no flow) conditions, 6-hour treatment with carrier-free S1P (f-S1P) induces a ~9.2-fold increase in L_p compared to untreated static control conditions. In comparison to treatment with f-S1P under static conditions, co-treatment of f-S1P with impinging bifurcated fluid flow (BFF) (~38 dyn•cm^{-2} stagnation pressure and approximately zero shear stress) at the base of the bifurcation point (BP) decreases L_p significantly. Similarly, co-stimulation of f-S1P with physiological levels of LSS (~3 dyn•cm^{-2}) in the branched vessel (BV) regions that are downstream of the BP also decreases L_p compared to f-S1P under static conditions. Furthermore, using pharmacological antagonists for S1PR1 (W146) and S1PR2 (JTE013), we show that flow-mediated stabilization of BFF and LSS is mediated by these two S1P receptors. The findings reported here demonstrate the importance of fluid mechanical cues at vessel bifurcations in coordinating S1P-mediated endothelial barrier function.

2. Results

2.1. Microfluidic model of a bifurcating vessel allows evaluation of S1P-dependent endothelial permeability

A biomimetic microfluidic model (Fig. 1) was fabricated using polydimethylsiloxane (PDMS) soft lithography, as previously reported [44, 45]. Briefly, this microfluidic model consists of an inlet channel that bifurcates around a central extracellular matrix (ECM) compartment separated by PDMS microposts to form two smaller, equally wide branched microchannels (Fig. 1A). The microfluidic model allows for the simultaneous application of BFF at the base of the BP, where the flow stagnates, and LSS in the branched vessels BV (Fig. 1Bi). Furthermore, the microfluidic device allows for direct contact between human umbilical vein endothelial cells (HUVECs) and abluminal 3-D collagen matrix at both the BP and the BV locations to examine the effect of the corresponding fluid forces on L_p (Fig. 1Bii, iii). The microchannels were uniformly lined with a monolayer of HUVECs (Fig. 1Ci), allowing for complete coverage of the ECM apertures at both BP and BV (Fig. 1Cii, iii). Moreover, the microfluidic platform enables controlled administration of S1P in the microchannels under both static and flow conditions.

2.2. Fluid mechanical forces associated with BFF and LSS attenuate endothelial permeability induced by carrier-free S1P

We first examined the effect of carrier-free S1P (f-S1P) on L_P under static or no-flow conditions in our microfluidic model. Previous studies have observed that S1P affects endothelial barrier function within 4–6 h of initial treatment [17, 46]. Treatment with 50 nM f-S1P for 6 h resulted in a 3.3-fold increase in L_P ($5.04 \times 10^{-4} \pm 1.00 \times 10^{-4}$ cm •s^{-1} •cmH_2O^{-1}, $p<0.01$) compared to the untreated and static condition ($1.51 \times 10^{-4} \pm 0.18 \times 10^{-4}$ cm•s^{-1} •cmH_2O^{-1}), henceforth referred to as baseline L_P (Figure S1). Moreover, treatment with 500 nM f-S1P for 6 h induced 9.2-fold increase in L_P ($13.88 \times 10^{-4} \pm$

2.54×10^{-4} cm •s^{-1} •cmH_2O^{-1}, $p<0.001$) compared to baseline L_P (Fig. S1; Fig. 2B, D). The observed increase in permeability of HUVECs with f-S1P at both tested concentrations (50 nM and 500 nM) compared to the untreated condition demonstrates a dose-dependent increase in L_P due to S1P treatment. Furthermore, the induced increase in permeability of HUVECs by f-S1P under static condition is supported by previous in vitro reports of the pro-angiogenic effects of f-S1P [11, 12].

Next, we examined the effects of co-stimulation of f-S1P with fluid flow on L_P at both the BP and BV apertures. These studies were done with 500 nM f-S1P because we observed the most potent increase in HUVEC L_P at this concentration under static conditions (Fig. S1). The media perfusion flow rate was adjusted to produce 3 dyn•cm–2 LSS in the BV regions of the microfluidic model, which is within the physiological range of shear stress in post-capillary venules (Fig. 2A) [47]. This flow rate of 10 μL/min generates a 38 dyn•cm^{-2} stagnation pressure with approximately zero average shear stress (Fig. 2A) as reported previously [44]. Compared to the 500 nM f-S1P treatment under static condition, co-application of 500 nM f-S1P with 38 dyn•cm^{-2} BFF for 6 h resulted in a significant decrease in L_P at the BP ($0.78 \times 10^{-4} \pm 0.24 \times 10^{-4}$ cm•s^{-1} •cmH_2O^{-1}, $p<0.01$) (Fig. 2B, D). Furthermore, the measured HUVEC L_P when co-treated with 500 nM f-S1P and 38 dyn•cm^{-2} BFF was not significantly different compared to treatment with 38 dyn•cm^{-2} BFF in the absence of S1P ($0.93 \times 10^{-4} \pm 0.16 \times 10^{-4}$ cm•s^{-1} •cmH_2O^{-1}) (Fig. 2B). Similar to the BP, co-application of 500 nM f-S1P with 3 dyn•cm^{-2} LSS for 6 h resulted in a significant decrease in L_P at the BV region ($0.87 \times 10^{-4} \pm 0.16 \times 10^{-4}$ cm•s^{-1} •cmH_2O^{-1}, $p<0.001$) compared to treatment with 500 nM f-S1P under static condition (Fig. 2B, D). Moreover, there was no significant difference in HUVEC L_P when co-stimulated with 3 dyn•cm^{-2} LSS and 500 nM f-S1P compared to 3 dyn•cm^{-2} LSS in the absence of S1P ($0.62 \times 10^{-4} \pm 0.25 \times 10^{-4}$ cm•s^{-1} •cmH_2O^{-1}) (Fig. 2B). These findings suggest that the fluid mechanical forces associated with 38 dyn•cm^{-2} BFF and 3 dyn•cm^{-2} LSS are endothelium-protective and counteract the induction of endothelial permeability due to f-S1P.

An important regulator of vascular permeability is the interendothelial junction protein VE-cadherin [48, 49]. Moreover, a previous study demonstrated the role of S1P in regulating the expression of VE-cadherin [21]. Therefore, we quantitatively examined VE-cadherin spatial expression using immunofluorescence and *en face* confocal microscopy images of the endothelial monolayers at the BP and BV apertures under different combinations of treatment with f-S1P and fluid forces (Fig. 2C). Intensity measurements of VE-cadherin immunofluorescence signal at HUVEC junctions did not show a significant difference in expression when treated with f-S1P under static or perfused conditions compared to the untreated control condition (Fig. 2C). These results suggest that the enhancement in endothelial barrier function due to BFF and LSS in the presence of f-S1P (Fig. 2B) was independent of VE-cadherin localization to inter-endothelial junctions (Fig. 2C).

2.3. Flow-mediated stabilization due to BFF and LSS is dependent on S1PR1 or S1PR2 signaling

Previous reports suggest that the effect of S1P on endothelial barrier function is dependent on the relative activation of S1PR1 and S1PR2 [9, 23, 50, 51]. These previous findings

prompted us to study the involvement of S1PR1 and S1PR2 in regulating BFF and LSS mediated vessel stabilization (Fig. 3A). We blocked S1P signaling with two widely used pharmacological antagonists with specificity for S1PR1 (W146) and S1PR2 (JTE013) [16, 23, 52, 53]. Under static conditions, pre-treatment with W146 followed by treatment with 500 nM f-S1P for 6 h in the presence of W146 resulted in a significant decrease in HUVEC L_P ($6.54 \times 10^{-4} \pm 1.53 \times 10^{-4}$ cm•s^{-1} •cmH_2O^{-1}, $p<0.05$) compared to the f-S1P treated condition without S1PR1 inhibition (Fig. 3Ai, Bi). This result suggests that S1PR1 activation by f-S1P contributes to the observed increase in vessel permeability under static conditions. This observation was surprising as multiple studies have highlighted the role of S1PR1 signaling in stabilizing the endothelium [19, 54]. Under the static condition, pre-treatment with JTE013 followed by treatment with 500 nM f-S1P for 6 h in the presence of JTE013 resulted in a more dramatic decrease in L_P ($1.08 \times 10^{-4} \pm 0.32 \times 10^{-4}$ cm•s^{-1} •cmH_2O^{-1}, $p<0.0001$) compared to the f-S1P treated condition with no inhibitor applied (Fig. 3Ai, Bi). This result is in accordance with previous reports that activation of S1PR2 induces S1P-mediated endothelial barrier destabilization [23].

In the BP region, pre-treatment with W146 or JTE013 followed by co-stimulation with 38 dyn•cm^{-2} BFF and 500 nM f-S1P in the presence of each receptor inhibitor for 6 h caused a significant increase in L_P compared to co-application of f-S1P with BFF for 6 h without receptor inhibition. W146: $4.71 \times 10{-4} \pm 0.86 \times 10^{-4}$ cm•s^{-1} •cmH_2O^{-1}, $p<0.01$ and JTE013: $3.79 \times 10^{-4} \pm 0.50 \times 10^{-4}$ cm•s^{-1} •cmH_2O^{-1}, $p<0.01$ (Fig. 3Aii, Bii). These results indicate that blocking either S1PR1 or S1PR2 signaling significantly affects BFF mediated vessel stabilization. Similarly, in the BV region, pre-treatment with W146 or JTE013 followed by co-application of 3 dyn•cm^{-2} LSS with 500 nM f-S1P for 6 h in the presence of each receptor inhibitor caused a significant increase in L_P compared to co-application of f-S1P with LSS for 6 h without receptor inhibition. W146: $5.88 \times 10^{-4} \pm 1.06 \times 10^{-4}$ cm•s^{-1} •cmH_2O^{-1}, $p<0.001$ and JTE013: $4.97 \times 10^{-4} \pm 1.03 \times 10^{-4}$ cm•s^{-1} •cmH_2O^{-1}, $p<0.01$ (Fig. 3Aiii, Biii). These results suggest that the enhancement in endothelial barrier function due to LSS is dependent on S1PR1 and S1PR2 signaling.

2.4. Association of S1P with albumin carrier transiently promotes vessel stabilization

The effects of S1P on vascular barrier function are known to be carrier dependent, and most studies of S1P bioactivity have employed albumin as the S1P carrier [55]. Therefore, we measured the effect on HUVECs L_P due to S1P reconstituted with bovine serum albumin (a-S1P) and compared the response with f-S1P under static conditions (Fig. 4). Treatment with 500 nM a-S1P for 6 h did not result in a significant difference in L_P ($1.69 \times 10^{-4} \pm 0.36 \times 10^{-4}$ cm•s^{-1} •cmH_2O^{-1}, $p>0.05$) compared to baseline L_P (Fig. 4A). However, the L_P measurement for a-S1P was ~88% lower than f-S1P at 6 h of treatment (1.69×10^{-4} versus 13.88×10^{-4} cm •s^{-1} •cmH_2O^{-1}, $p<0.0001$; Fig. 4A, B). These results demonstrate clearly that the effects of S1P on L_P are dependent on association with albumin as a carrier molecule. It is noted that the preparation of f-S1P and a-S1P stock solutions require different buffer conditions (see the Materials and Methods). We performed a set of control experiments and confirmed that the differential effects of f-S1P and a-S1P on HUVEC L_P were not due to the difference in preparation buffers (Fig. S2).

Next, we studied the effects of co-treatment of a-S1P with BFF and LSS on HUVEC L_P at the BP and BV apertures, respectively. At the BP, co-application of 500 nM a-S1P with 38 dyn•cm^{-2} BFF for 6 h did not cause a significant change in L_P ($2.71 \times 10^{-4} \pm 0.53 \times 10^{-4}$ cm•s^{-1} •cmH_2O^{-1}) compared to the 500 nM a-S1P treatment for 6 h under static conditions (Fig. 4A). Furthermore, HUVEC L_P due to 38 dyn•cm^{-2} BFF in the absence of S1P ($0.93 \times 10^{-4} \pm 0.16 \times 10^{-4}$ cm•s^{-1} •cmH_2O^{-1}) was significantly lower compared to co-treatment with 38 dyn•cm^{-2} BFF and 500 nM a-S1P ($2.71 \times 10^{-4} \pm 0.53 \times 10^{-4}$ cm•s^{-1} •cmH_2O^{-1}) (Fig. 4A). At the BV, co-application of 500 nM a-S1P with 3 dyn•cm^{-2} LSS for 6 h did not show a significant difference in L_P ($1.73 \times 10^{-4} \pm 0.27 \times 10^{-4}$ cm•s^{-1} •cmH_2O^{-1}) compared to treatment with 500 nM a-S1P under static condition (Fig. 4A). In contrast, there was a significant decrease in HUVEC L_P when stimulated with 3 dyn•cm^{-2} LSS in the absence of a-S1P ($0.62 \times 10^{-4} \pm 0.25 \times 10^{-4}$ cm•s^{-1} •cmH_2O^{-1}) compared to 3 dyn•cm^{-2} LSS and 500 nM a-S1P ($1.73 \times 10^{-4} \pm 0.27 \times 10^{-4}$ cm•s $^{-1}$ •cmH_2O $^{-1}$) (Fig. 4A).

We also measured HUVECs L_P due to treatment with a-S1P or f-S1P for 1 hour under static conditions. These experiments were motivated by previous reports demonstrating that the effects of S1P on endothelial permeability are time-dependent [17, 46]. For instance, treatment with a-S1P (150–500 nM) under static conditions caused a peak in the transendothelial impedance, which was indicative of enhanced endothelial barrier function, within 30–60 min [17, 46]. This response was followed by a steady decline in barrier function that equilibrated to control levels by 4–5 h [17, 46]. Our observed HUVECs L_P measurements at 1 hour and 6 h of a-S1P treatment under static conditions were in accordance with these previously reported time-dependent measurements of transendothelial electrical resistance for endothelial barrier integrity [56]. While treatment with 500 nM a-S1P for 1 hour under static conditions caused a significant decrease in L_P ($0.69 \times 10^{-4} \pm 0.22 \times 10^{-4}$ cm •s^{-1} •cmH_2O^{-1}, $p<0.05$) compared to baseline L_P, the same treatment conditions for 6 h resulted in no difference in L_P compared to baseline L_P (Fig. 4A). In contrast to a-S1P, treatment with 500 nM f-S1P for 1 hour under static conditions did not elicit a significant change in L_P ($1.46 \times 10^{-4} \pm 0.13 \times 10^{-4}$ cm•s^{-1} •cmH_2O^{-1}, $p>0.05$) compared to baseline L_P (Fig. 4A). Therefore, L_P for a-S1P was ~48% lower than f-S1P at 1 hour of treatment (0.76×10^{-4} versus 1.46×10^{-4} cm •s^{-1} •cmH_2O^{-1} respectively, $p<0.05$; Fig. 4A, B).

Next, we examined the role of S1PR1 and S1PR2 in mediating the vessel stabilization effects of 1 hour of a-S1P treatment under static conditions. Selective inhibition of S1PR1 signaling with pretreatment of W146 followed by treatment with 500 nM a-S1P for 1 hour in the presence of W146 abrogated the stabilizing effect of a-S1P ($2.05 \times 10^{-4} \pm 0.78 \times 10^{-4}$ cm•s^{-1} •cmH_2O^{-1}, $p<0.05$) (Fig. 4C). In contrast, blocking S1PR2 signaling with JTE013 followed by treatment with 500 nM a-S1P for 1 hour in the presence of JTE013 did not significantly impact the stabilizing effect of a-S1P ($1.26 \times 10^{-4} \pm 0.30 \times 10^{-4}$ cm •s^{-1} •cmH_2O^{-1}, $p>0.05$) (Fig. 4C). These findings suggest that time-dependent vessel stabilization induced by a-S1P treatment (Fig. 4A, B) requires S1PR1 but not S1PR2 signaling.

3. Discussion

Laminar shear stress (LSS) due to blood flow has been reported to influence S1P signaling to the endothelium [36]. However, vascular networks are comprised of branching structures, which generate hemodynamic forces distinct from LSS. At the base of vessel bifurcations, blood flow generates bifurcated fluid flow (BFF) which results in a finite stagnation pressure and near-zero average shear stress. Yet, the role of BFF and LSS in mediating the effects of f-S1P on endothelial permeability remains largely unstudied in in vivo vascular models because of the challenges in controlling hemodynamic factors and biomolecular conditions while deriving quantifiable metrics for vascular barrier function. Here, we provided a deeper understanding of how the flow dynamics associated with blood vessel bifurcations coordinate S1P-mediated vessel permeability. These studies were enabled by the capabilities of our recently reported microfluidic model of vessel bifurcations, which provides quantitative measurements of the vessel permeability coefficient (L_P) in response to well-controlled levels of BFF and LSS [44].

While carrier-bound S1P is known to be a vasoprotective and atheroprotective factor [19, 20], previous studies have shown that carrier-free S1P (f-S1P) promotes compromised barrier function associated with inflammation and atherogenesis [25, 27]. Moreover, elevated levels of extravascular-borne f-S1P have been linked to increased destabilization of the tumor vasculature and is a promoter of pulmonary inflammation [57, 58]. As a baseline, we measured vessel permeability due to treatment with f-S1P under static conditions, where we observed a potent induction in HUVEC permeability. This observation was in accordance with previous reports on the role of f-S1P in promoting inflammatory responses in ECs [26, 27] and angiogenic sprouting [12]. When f-S1P is co-applied with BFF and LSS, however, we observed a significant decrease in HUVEC permeability compared to the condition when f-S1P is applied under static conditions. These findings highlighted the prominent role of both BFF and LSS in suppressing the induction of vessel permeability by f-S1P. These observations were in agreement with our previous report on the vessel stabilizing effects of BFF and LSS compared to the static untreated condition [44].

While there is evidence for S1P-induced assembly of VE-cadherin adherens junctions [21]. S1P has also been shown to transiently enhance the endothelial barrier integrity through Rho-dependent cell spreading that is independent of VE-cadherin binding [59]. Our present findings suggest that f-S1P induced changes in HUVEC L_P under static or perfused condition are not dependent on VE-cadherin expression. However, further studies are needed to reveal the mechanism responsible for f-S1P dependent alterations in adherens junction structure that manifest changes in endothelial permeability.

A key area of interest in endothelial mechanosensing is identifying signaling molecules that are regulated by mechanical forces (i.e., mechanosensors). For instance, we previously reported that the decreases in endothelial permeability caused by BFF and LSS were both dependent on the nitric oxide (NO) signaling pathway [44]. However, the mechanisms by which ECs discern different physical forces (e.g., BFF and LSS) are not known. Thus, a major finding from our study is that vessel stabilization due to BFF and LSS is dependent on S1PR1 or S1PR2. Under perfusion, selectively blocking either S1PR1 or S1PR2 signaling

caused a significant increase in HUVEC L_P in response to co-treatment with f-S1P and BFF. Similarly, under LSS, blocking either S1PR1 or S1PR2 signaling caused a significant increase in L_P. Previous in vivo observations on vascular hyper-sprouting in S1PR1 knock-out mice support our observation on increased L_P in response to co-stimulation with f-S1P and LSS at BV if S1PR1 signaling is blocked [36, 60]. However, these in vivo observations did not distinguish between regions of elevated LSS versus vessel bifurcation points in terms of level of hyper-sprouting. Moreover, while endothelial S1PR1 has been implicated as mechanosensitive to LSS in promoting vessel stabilization [36], our findings suggest a novel mechanosensitive role for S1PR1 in response to BFF along with S1PR2 in response to BFF and LSS in coordinating endothelial barrier function.

Blood flow (i.e., LSS) enhances transcription and expression of S1PR1 [34, 36], and there is evidence of ligand independent activation of S1PR1 that leads to vessel stabilization [36]. However, there are no previous reports that address whether BFF elicits ligand independent activation of S1PR1. Interestingly, a recent study on the transcriptomics of adult mouse aortic endothelial cells reported ligand-independent coupling of S1PR1 and β-arrestin at vascular branching points [61]. Furthermore, HDL-S1P is shown to induce increased S1PR1/β-arrestin coupling [20] and is endothelium-protective [19], suggesting that the observed ligand-independent coupling of S1PR1 and β-arrestin is due to activation and recycling of S1PR1 in response to branching point hemodynamics. Therefore, further studies are required to elucidate the mechanism by which LSS and BFF inhibit vessel destabilization by f-S1P. In addition, we note that in contrast to our findings, there are previous reports of combined S1P treatment and LSS inducing angiogenic sprouting [62, 63], which is often associated with destabilization of the endothelial monolayer [8]. Yet, it is important to consider that these observations were based on higher levels of LSS (> ~6 dyn•cm^{-2}) compared to the results reported here. Thus, our findings demonstrate that the magnitude of hemodynamic forces should be considered when evaluating the effects on S1P-dependent vascular permeability.

Previous studies have highlighted the essential role of protein carriers for S1P (e.g., albumin or HDL) in regulating S1PR1-mediated endothelial barrier integrity [64]. These carriers can engage specific endothelial co-receptors, which are not activated when treated with f-S1P [64]. Therefore, we also compared the effect of f-S1P on HUVEC L_P to when S1P is associated with albumin carrier (a-S1P). In contrast with the observed increase in L_P induced by f-S1P, treatment with a-S1P under static condition caused a transient enhancement of the HUVEC barrier that returned to baseline levels after 6 h. Furthermore, enhancement of HUVEC barrier by a-S1P was mediated by S1PR1 signaling and was independent of S1PR2 signaling. These findings suggest biased activation of S1PR1 over S1PR2 by a-S1P, which is in agreement with previously reported dependence of S1P signaling on its carrier [65]. Furthermore, presence of a sharp transvascular gradient of S1P under physiological condition has been linked to the role of S1P in modulating endothelial permeability via a dynamic S1PR1 signaling model when activated abluminally [66]. Since a-S1P is significantly larger in size compared to f-S1P (by ~2 order of magnitude), luminal administration of a-S1P in the implemented microfluidic device results in a sharp transendothelial gradient that is more sustainable compared when S1P was administered without a carrier. Future studies will determine whether the observed effects of fluid forces and a-S1P can be extended to the corresponding conditions with HDL-S1P.

ECs are known to express S1PR3 in addition to S1PR1 and S1PR2 [10]. However, the contribution of S1PR3 in coordinating S1P-regulated endothelial barrier function is less clear compared to S1PR1 and S1PR2 [10, 67]. Some in vivo [68, 69] and in vitro [21, 70] evidence indicate a supportive role for S1PR3 in protecting endothelial barrier integrity alongside S1PR1. This role for S1PR3 may explain our observation that HUVECs under static conditions that were pretreated with W146 for S1PR1 antagonism experienced a decrease in L_P, even though S1PR1 is believed to stabilize the endothelium. Functional overlap and partial redundant activity by S1PR3 may promote a decrease the HUVEC L_P despite antagonism of S1PR1 activity. Furthermore, further studies on selective S1PR3 signaling can help elucidate its potential role in coordinating hemodynamic cues exerted by BFF and LSS on ECs.

In terms of the pathophysiological relevance of our findings, it is well established that flow patterns in tumor associated vasculature are highly abnormal with regions of low flow or flow stasis [71, 72]. For instance, Yuan et al. showed that maximum velocity in tumor-free pial venules is one to three orders of magnitude greater than the maximum velocity in tumor-associated vessels of comparable diameter [73]. It is worth noting that the estimated Reynolds (*Re*) number in the tumor-free pial venules was ~0.3 [73], which is similar to the *Re* number in the BV region (~0.2) in the microvessel analogue here. Furthermore, heightened sphingosine kinase activation is present in the cells of the tumor microenvironment, which results in upregulation of stroma-derived and perivascular-borne S1P [74]. Therefore, our findings suggest that the absence of ordered and physiological hemodynamic conditions in the tumor-associated vasculature combined with elevated S1P from the tumor stroma may be contributing factors to pathological angiogenesis.

4. Conclusion

The work here presents to our knowledge the first report on the importance of hemodynamic forces associated with vessel bifurcations (i.e., BFF and LSS) in regulating S1P-mediated vascular barrier function. Moreover, our findings provide insights on the role of S1PR1 and S1PR2 in coordinating changes in HUVEC L_P induced by f-S1P. These findings were enabled by the versatility of the described in vitro microfluidic model. Future studies using this model will further enhance the understanding of hemodynamic forces in co-regulating S1P signaling, with potential relevance to vascular barrier function and protection against inflammatory, atherogenic, and oncogenic disorders.

5. Materials and methods

5.1. Chemical reagents

To prepare stock solution of sphingosine-1-phosphate (S1P), S1P (Cayman) was dissolved in 1X Dulbecco's phosphate-buffered saline (DPBS) (Corning) with 0.3 M NaOH (Sigma-Aldrich) at 10 mM. To make stock solution of S1P associated with fatty acid-free Bovine Serum Albumin (BSA) (Sigma) carrier proteins, S1P (Avanti Polar Lipids) was resuspended in a methanol: water solution (95:5 volumetric ratio) and heated to 65 °C with sonication to form a 0.5 mg mL^{-1} S1P solution. This solution was then dried with dry nitrogen stream. The dried S1P residue was dissolved in 1X PBS with 4 $mgmL^{-1}$ fatty acid free BSA to

a final concentration of 125 μM S1P. Stock solution of W146 (Cayman) was prepared by dissolving in DMSO at 50 mM. Stock solution of JTE-013 (Cayman) was prepared by dissolving in DMSO at 10 mM.

5.2. Microfluidic platform

The microfluidic platform was fabricated and implemented as previously described[44]. Briefly, the microfluidic device consists of a 1300 μm wide main channel that symmetrically branches into two downstream microchannels that are 500 μm in width. Moreover, the main channel branches around a central extracellular matrix compartment (400 μm wide) that encloses the collagenous hydrogel while allowing for direct interaction between the endothelial cells seeded in the channel network and the collagen matrix at the base of the bifurcation point and within the branching microchannels. Direct contact between ECs and collagen matrix was enabled by the 100 μm wide gaps in the PDMS barrier (referred to as apertures) that separates the ECM compartment from the microchannels. To form individual microfluidic devices, polydimethylsiloxane (PDMS) solution was prepared by mixing silicon elastomer base and curing agent (Ellsworth Adhesives) at a weight ratio of 10:1 and was cast on a silicon master that featured the 50 μm in height monolithic microfluidic patterns microfabricated using SU-8 photolithography. The PDMS microdevices were irreversibly bonded on glass slides using plasma treatment and sterilized with UV light prior to casting the collagenous hydrogel.

5.3. Type I collagen hydrogel preparation

The 3-D extracellular matrix (ECM) was comprised of a 3 $mg.mL^{-1}$ collagen type I from rat tail (Corning) solution that was casted and polymerized within the central compartment of the microdevice. A basic solution was prepared using 10X DPBS (Thermo Fisher) and 1 M NaOH (Sigma-Aldrich) to titrate the collagen solution pH to 7.4. To facilitate the adhesion of the endothelial cells and formation of a confluent monolayer on each ECM interface, the collagenous solution was supplemented with human fibronectin (Corning) to a final concentration of 10 $\mu g\ mL^{-1}$ fibronectin. The final 3 $mg\ mL^{-1}$ collagenous solution with pH≈7.4 was incubated on ice for ~10 min prior to injection into the ECM microchannel. Following the injection, the cast microdevices were incubated at 37 °C to enable proper polymerization of the collagen fibers.

5.4. Preparation of HUVECs

Human umbilical vein endothelial cells (HUVECs) (Lonza) were cultured using endothelial growth media (EGM) (Lonza) in a cell culture incubator at 37 °C with 5% CO_2. To seed the microdevices, HUVECs (passage numbers between 5 and 10) were rinsed with 1X DPBS without Mg/Ca (Thermo Fisher), followed by incubation with 0.05% Trypsin-EDTA (Thermo Fisher) for 45 s at 37 °C to detach the ECs from the cell culture flask. The detached cells were re-suspended in fresh EGM and prepared for seeding the microdevices. The microdevices that included the polymerized collagen matrix were flushed with 10 μgmL^{-1} human fibronectin solution (Corning) diluted in 1X DPBS and incubated for 90 min at 37 °C. Fibronectin-coated microfluidic channels were then flushed with EGM and incubated overnight at 37 °C prior to seeding the HUVECs into the perfusion channels. The HUVECs were removed from the cell culture flask with trypsin and re-suspended in EGM at ~

40,000 cells μL^{-1}. The microfluidic channels were then injected with the cell suspension and incubated overnight at 37 °C to facilitate the formation of microdevices fully coated with HUVEC monolayer.

5.5. Pharmacological antagonization of S1P receptors

To pharmacologically antagonize S1P receptor 1, the microfluidic devices seeded with HUVECs were incubated with EGM supplemented with 10 μM W146 for 3 h at 37 °C [16] followed by treatment under each experimental test condition in the presence of 10 μM W146. To pharmacologically antagonize S1P receptor 2, the microdevices seeded with HUVECs were incubated with EGM supplemented with 200 nM JTE-013 for 30 min at 37 °C [23]. The devices were then treated under each experimental test condition in the presence of 200 nM JTE013.

5.6. Immunofluorescence

Microfluidic devices were flushed three times with 1X DPBS and incubated with 4% paraformaldehyde (Sigma-Aldrich) in 1X PBS for 20 min at room temperature following each experimental test condition. The microfluidic devices were then flushed 3 times with 1X DPBS and incubated with blocking buffer, which consists of 5% BSA (Sigma-Aldrich) and 0.1% Triton X-100 (Sigma-Aldrich) for 1 hour. Next, the devices were rinsed 3 times with 1X DPBS, and incubated for 90 min with Alexa647 conjugated anti-human VE-cadherin primary antibody (Life Sciences). Then, the devices were flushed 3 times with 1X DPBS followed by incubation with DAPI (Sigma-Aldrich) diluted in double distilled water by 1:1000 for 3 min to stain for HUVEC nuclei. The devices were finally flushed 3 times with 1X PBS prior to imaging.

For quantitative examination of VE-cadherin immunofluorescence signal, five cross-sectional confocal images at 15 μm, 20 μm, 25 μm, 30 μm, and 35 μm vertical distance from the glass coverslip at each aperture were analyzed. Using previously reported methods [75, 76], we developed a custom MATLAB code where the VE-cadherin signal was recorded along the interface between the ECM and the HUVEC monolayer for each confocal image. Regions along the interface were manually highlighted as junctional sections based on visual examination of each confocal image. The recorded fluorescence signal intensity along the selected junctional regions was averaged and reported as the representative immunofluorescence intensity per confocal image [76]. The average fluorescence intensity values at HUVEC junctions per confocal image were presented as scatter plots with the average intensity denoted with a line (Fig. 2C).

5.7. Image acquisition

Before and after treatment under each condition, the HUVECs were imaged using phase contrast imaging. Furthermore, epifluorescence imaging was performed using epifluorescence microscopy (473 nm excitation / 488 nm emission, TS100, Nikon) with a 10X air objective to monitor the transendothelial transport of FITC conjugated 10 kDa Dextran (Sigma Aldrich). Timelapse epifluorescence imaging was performed at 1 s intervals for up to 5 min to capture the dynamic transendothelial transport of the fluorescent tracer. The timelapse epifluorescence images were analyzed using MATLAB to quantify

endothelial hydraulic conductivity as previously reported [44]. Confocal microscopy was performed on the stained microdevices using a laser scanning confocal scope (A1R, Nikon) with a 40X oil immersion objective to examine the interendothelial junction structure at the bifurcation point (BP) and in each branched vessel (BV) aperture. A laser type light source was used to excite DAPI (blue) and Alexa 647 conjugated VE-cadherin antibody (far red). VE-cadherin expression at each aperture was examined *en face* by reconstituting a 3-D rendering of the immunofluorescence signal based on multiple confocal images (0.5 μm per image slice).

5.8. Statistical analysis

Numerical values reported in the results section represent the mean ± the standard error of the mean. Each test condition was repeated using at least three microdevices. Two-sided student t-tests were used to report the statistical significance between each pair of experimental test condition for L_P. Levels of significance were reported using the following: * indicates $p\text{-}value < 0.05$, ** indicates $p\text{-}value < 0.01$, and *** indicates $p\text{-}value < 0.001$.

Supplementary Material

Refer to Web version on PubMed Central for supplementary material.

Acknowledgements

This work was supported by the National Heart Lung Blood Institute (R01HL141941), American Heart Association (15SDG25480000), The Mark Foundation for Cancer Research ASPIRE Award, and the Center for Emergent Materials, an NSF-MRSEC, grant DMR-1420451, the Center for Exploration of Novel Complex Materials, and the Institute for Materials Research. E.A. and K.K.R acknowledge OSU Presidential Fellowships. G.B.S. acknowledges funding from the Undergraduate Summer Research Program of The American Heart Association Great Rivers Affiliate, a Barry M. Goldwater Scholarship, and an Ohio State University (OSU) Comprehensive Cancer Center Pelotonia Fellowship. M.M.M. acknowledges funding from an Ohio State University (OSU) Comprehensive Cancer Center Pelotonia Fellowship. The authors acknowledge the OSU Campus Microscopy and Imaging Facility (CMIF) for assistance with confocal microscopy. This facility is supported in part by grant P30 CA016058 from the NCI. We thank Peter Beshay, Chia-Wen Chang, and Jonathan Adorno for helpful discussions.

References

[1]. Bazzoni G, Dejana E. Endothelial cell-to-cell junctions: molecular organization and role in vascular homeostasis. Physiol Rev 2004;84(3):869–901. [PubMed: 15269339]

[2]. Cerutti C, Ridley AJ. Endothelial cell-cell adhesion and signaling. Exp Cell Res 2017;358(1):31–8. [PubMed: 28602626]

[3]. Michel C, Curry F. Microvascular permeability. Physiol Rev 1999;79(3):703–61. [PubMed: 10390517]

[4]. McDonald DM. Endothelial Gaps: plasma Leakage During Inflammation. News Physiol Sci 1998;13(2):104–5. [PubMed: 11390771]

[5]. Tarbell JM. Mass transport in arteries and the localization of atherosclerosis. Annu Rev Biomed Eng 2003;5(1):79–118. [PubMed: 12651738]

[6]. Stylianopoulos T, Munn LL, Jain RK. Reengineering the Physical Microenvironment of Tumors to Improve Drug Delivery and Efficacy: from Mathematical Modeling to Bench to Bedside. Trends Cancer 2018;4(4):292–319. [PubMed: 29606314]

[7]. Park-Windhol C, D'Amore PA. Disorders of Vascular Permeability. Annu Rev Pathol 2016;11:251–81. [PubMed: 26907525]

[8]. Nagy JA, Benjamin L, Zeng H, Dvorak AM, Dvorak HF. Vascular permeability, vascular hyperpermeability and angiogenesis. AngiogenesisAngiogenesis 2008;11(2):109–19.

[9]. Cartier A, Hla T. Sphingosine 1-phosphate: lipid signaling in pathology and therapy. ScienceScience 2019;366(6463):eaar5551.

[10]. Xiong Y, Hla T, S1P control of endothelial integrity. Curr Top Microbiol Immunol 2014;378:85–105. [PubMed: 24728594]

[11]. Bayless KJ, Davis GE. Sphingosine-1-phosphate markedly induces matrix metalloproteinase and integrin-dependent human endothelial cell invasion and lumen formation in three-dimensional collagen and fibrin matrices. Biochem Biophys Res Commun 2003;312(4):903–13. [PubMed: 14651957]

[12]. Nguyen DH, Stapleton SC, Yang MT, Cha SS, Choi CK, Galie PA, Chen CS, Biomimetic model to reconstitute angiogenic sprouting morphogenesis in vitro. Proc Natl Acad Sci U S A 2013;110(17):6712–17. [PubMed: 23569284]

[13]. English D, Kovala AT, Welch Z, Harvey KA, Siddiqui RA, Brindley DN, Garcia JG, Induction of endothelial cell chemotaxis by sphingosine 1-phosphate and stabilization of endothelial monolayer barrier function by lysophosphatidic acid, potential mediators of hematopoietic angiogenesis. J Hematother Stem Cell Res 1999;8(6):627–34. [PubMed: 10645770]

[14]. Graeler M, Shankar G, Goetzl EJ. Cutting edge: suppression of T cell chemotaxis by sphingosine 1-phosphate. J Immunol 2002;169(8):4084–7. [PubMed: 12370333]

[15]. Jozefczuk E, Guzik TJ, Siedlinski M. Significance of sphingosine-1-phosphate in cardiovascular physiology and pathology. Pharmacol Res 2020;156:104793. [PubMed: 32278039]

[16]. Sanna MG, Wang SK, Gonzalez-Cabrera PJ, Don A, Marsolais D, Matheu MP, Wei SH, Parker I, Jo E, Cheng WC, Cahalan MD, Wong CH, Rosen H. Enhancement of capillary leakage and restoration of lymphocyte egress by a chiral S1P1 antagonist in vivo. Nat Chem Biol 2006;2(8):434–41. [PubMed: 16829954]

[17]. Wilkerson BA, Grass GD, Wing SB, Argraves WS, Argraves KM. Sphingosine 1-phosphate (S1P) carrier-dependent regulation of endothelial barrier: high density lipoprotein (HDL)-S1P prolongs endothelial barrier enhancement as compared with albumin-S1P via effects on levels, trafficking, and signaling of S1P1. J Biol Chem 2012;287(53):44645–53. [PubMed: 23135269]

[18]. Murata N, Sato K, Kon J, Tomura H, Yanagita M, Kuwabara A, Ui M, Okajima F. Interaction of sphingosine 1-phosphate with plasma components, including lipoproteins, regulates the lipid receptor-mediated actions. Biochem J 352 Pt 2000;3(3):809–15.

[19]. Christoffersen C, Obinata H, Kumaraswamy SB, Galvani S, Ahnstrom J, Sevvana M, Egerer-Sieber C, Muller YA, Hla T, Nielsen LB, Dahlback B. Endothelium-protective sphingosine-1-phosphate provided by HDL-associated apolipoprotein M. Proc Natl Acad Sci U S A 2011;108(23):9613–18. [PubMed: 21606363]

[20]. Galvani S, Sanson M, Blaho VA, Swendeman SL, Obinata H, Conger H, Dahlback B, Kono M, Proia RL, Smith JD, Hla T, HDL-bound sphingosine 1-phosphate acts as a biased agonist for the endothelial cell receptor S1P1 to limit vascular inflammation. Sci Signal 2015;8(389):ra79. [PubMed: 26268607]

[21]. Lee MJ, Thangada S, Claffey KP, Ancellin N, Liu CH, Kluk M, Volpi M, Sha'afi RI, Hla T. Vascular endothelial cell adherens junction assembly and morphogenesis induced by sphingosine-1-phosphate. CellCell 1999;99(3):301–12.

[22]. Singleton PA, Dudek SM, Chiang ET, Garcia JG. Regulation of sphingosine 1-phosphate-induced endothelial cytoskeletal rearrangement and barrier enhancement by S1P1 receptor, PI3 kinase, Tiam1/Rac1, and alpha-actinin. FASEB J 2005;19(12):1646–56. [PubMed: 16195373]

[23]. Sanchez T, Skoura A, Wu MT, Casserly B, Harrington EO, Hla T, Induction of vascular permeability by the sphingosine-1-phosphate receptor-2 (S1P2R) and its downstream effectors ROCK and PTEN. Arterioscler Thromb Vasc Biol 2007;27(6):1312–18. [PubMed: 17431187]

[24]. Kon J, Sato K, Watanabe T, Tomura H, Kuwabara A, Kimura T, Tamama K, Ishizuka T, Murata N, Kanda T, Kobayashi I, Ohta H, Ui M, Okajima F, Comparison of intrinsic activities of the putative sphingosine 1-phosphate receptor subtypes to regulate several signaling pathways in their cDNA-transfected Chinese hamster ovary cells. J Biol Chem 1999;274(34):23940–7. [PubMed: 10446161]

[25]. Sattler K, Levkau B. Sphingosine-1-phosphate as a mediator of high-density lipoprotein effects in cardiovascular protection. Cardiovasc Res 2009;82(2):201–11. [PubMed: 19233866]

[26]. Xia P, Gamble JR, Rye KA, Wang L, Hii CS, Cockerill P, Khew-Goodall Y, Bert AG, Barter PJ, Vadas MA, Tumor necrosis factor-alpha induces adhesion molecule expression through the sphingosine kinase pathway. Proc Natl Acad Sci U S A 1998;95(24):14196–201. [PubMed: 9826677]

[27]. Zhang G, Yang L, Kim GS, Ryan K, Lu S, O'Donnell RK, Spokes K, Shapiro N, Aird WC, Kluk MJ, Yano K, Sanchez T. Critical role of sphingosine-1-phosphate receptor 2 (S1PR2) in acute vascular inflammation. BloodBlood 2013;122(3):443–55.

[28]. Pyne NJ, Pyne S. Sphingosine 1-phosphate and cancer. Nat Rev Cancer 2010;10(7):489–503. [PubMed: 20555359]

[29]. Visentin B, Vekich JA, Sibbald BJ, Cavalli AL, Moreno KM, Matteo RG, Garland WA, Lu Y, Yu S, Hall HS. Validation of an anti-sphingosine-1-phosphate antibody as a potential therapeutic in reducing growth, invasion, and angiogenesis in multiple tumor lineages. Cancer Cell 2006;9(3):225–38. [PubMed: 16530706]

[30]. Nagahashi M, Ramachandran S, Kim EY, Allegood JC, Rashid OM, Yamada A, Zhao R, Milstien S, Zhou H, Spiegel S, Takabe K. Sphingosine-1-phosphate produced by sphingosine kinase 1 promotes breast cancer progression by stimulating angiogenesis and lymphangiogenesis. Cancer Res 2012;72(3):726–35. [PubMed: 22298596]

[31]. Gimbrone MA Jr, Garcia-Cardena G. Vascular endothelium, hemodynamics, and the pathobiology of atherosclerosis. Cardiovasc Pathol 2013;22(1):9–15 [PubMed: 22818581]

[32]. Gordon E, Schimmel L, Frye M, The Importance of Mechanical Forces for in vitro Endothelial Cell Biology. Front Physiol 2020;11:684. [PubMed: 32625119]

[33]. Tarbell JM. Shear stress and the endothelial transport barrier. Cardiovasc Res 2010;87(2):320–30. [PubMed: 20543206]

[34]. Takada Y, Kato C, Kondo S, Korenaga R, Ando J. Cloning of cDNAs encoding G protein-coupled receptor expressed in human endothelial cells exposed to fluid shear stress. Biochem Biophys Res Commun 1997;240(3):737–41. [PubMed: 9398636]

[35]. Aoki S, Osada M, Kaneko M, Ozaki Y, Yatomi Y. Fluid shear stress enhances the sphingosine 1-phosphate responses in cell–cell interactions between platelets and endothelial cells. Biochem Biophys Res Commun 2007;358(4):1054–7. [PubMed: 17512899]

[36]. Jung B, Obinata H, Galvani S, Mendelson K, Ding BS, Skoura A, Kinzel B, Brinkmann V, Rafii S, Evans T, Hla T. Flow-regulated endothelial S1P receptor-1 signaling sustains vascular development. Dev Cell 2012;23(3):600–10. [PubMed: 22975328]

[37]. Ghaffari S, Leask RL, Jones EA. Simultaneous imaging of blood flow dynamics and vascular remodelling during development. Development 2015;142(23):4158–67. [PubMed: 26443647]

[38]. Gray KM, Stroka KM, Vascular endothelial cell mechanosensing: new insights gained from biomimetic microfluidic models. Semin Cell Dev Biol 2017;71:106–17. [PubMed: 28633977]

[39]. Griffith CM, Huang SA, Cho C, Khare TM, Rich M, Lee G-h, Ligler FS, Diekman BO, Polacheck WJ. Microfluidics for the study of mechanotransduction. J Phys D Appl Phys 2020;53(22):224004. [PubMed: 33840837]

[40]. Pradhan S, Banda OA, Farino CJ, Sperduto JL, Keller KA, Taitano R, Slater JH, Bio-fabrication Strategies and Engineered In Vitro Systems for Vascular Mechanobiology. Adv Healthc Mater 2020;9(8):e1901255. [PubMed: 32100473]

[41]. Wong KH, Chan JM, Kamm RD, Tien J. Microfluidic models of vascular functions. Annu Rev Biomed Eng 2012;14(1):205–30. [PubMed: 22540941]

[42]. Das A, Tanner S, Barker DA, Green D, Botchwey EA, Delivery of S1P receptor-targeted drugs via biodegradable polymer scaffolds enhances bone regeneration in a critical size cranial defect. J Biomed Mater Res A 2014;102(4):1210–18. [PubMed: 23640833]

[43]. Akbari E, Spychalski GB, Song JW. Microfluidic approaches to the study of angiogenesis and the microcirculation. Microcirculation 2017;24(5).

[44]. Akbari E, Spychalski GB, Rangharajan KK, Prakash S, Song JW. Flow dynamics control endothelial permeability in a microfluidic vessel bifurcation model. Lab Chip 2018;18(7):1084–93. [PubMed: 29488533]

[45]. Akbari E, Spychalski GB, Rangharajan KK, Prakash S, Song JW. Competing Fluid Forces Control Endothelial Sprouting in a 3-D Microfluidic Vessel Bifurcation Model. Micromachines (Basel) 2019;10(7):451.

[46]. Argraves KM, Gazzolo PJ, Groh EM, Wilkerson BA, Matsuura BS, Twal WO, Hammad SM, Argraves WS, High density lipoprotein-associated sphingosine 1-phosphate promotes endothelial barrier function. J Biol Chem 2008;283(36):25074–81. [PubMed: 18606817]

[47]. Aird WC. Spatial and temporal dynamics of the endothelium. J Thromb Haemost 2005;3(7):1392–406. [PubMed: 15892866]

[48]. Giannotta M, Trani M, Dejana E. VE-cadherin and endothelial adherens junctions: active guardians of vascular integrity. Dev Cell 2013;26(5):441–54. [PubMed: 24044891]

[49]. Mehta D, Malik AB. Signaling mechanisms regulating endothelial permeability. Physiol Rev 2006;86(1):279–367. [PubMed: 16371600]

[50]. Bigaud M, Guerini D, Billich A, Bassilana F, Brinkmann V. Second generation S1P pathway modulators: research strategies and clinical developments. Biochim Biophys Acta 2014;1841(5):745–58. [PubMed: 24239768]

[51]. Prager B, Spampinato SF, Ransohoff RM, Sphingosine 1-phosphate signaling at the blood–brain barrier. Trends Mol Med 2015;21(6):354–63 [PubMed: 25939882]

[52]. Blaho VA, Hla T. An update on the biology of sphingosine 1-phosphate receptors. J Lipid Res 2014;55(8):1596–608. [PubMed: 24459205]

[53]. Osada M, Yatomi Y, Ohmori T, Ikeda H, Ozaki Y, Enhancement of sphingosine 1-phosphate-induced migration of vascular endothelial cells and smooth muscle cells by an EDG-5 antagonist. Biochem Biophys Res Commun 2002;299(3):483–7. [PubMed: 12445827]

[54]. Swendeman SL, Xiong Y, Cantalupo A, Yuan H, Burg N, Hisano Y, Cartier A, Liu CH, Engelbrecht E, Blaho V, Zhang Y, Yanagida K, Galvani S, Obinata H, Salmon JE, Sanchez T, Di Lorenzo A, Hla T, An engineered S1P chaperone attenuates hypertension and ischemic injury. Sci Signal 2017;10(492).

[55]. Wilkerson BA, Argraves KM, The role of sphingosine-1-phosphate in endothelial barrier function. Biochim Biophys Acta 2014;1841(10):1403–12. [PubMed: 25009123]

[56]. Bogorad MI, DeStefano J, Karlsson J, Wong AD, Gerecht S, Searson PC, Review: in vitro microvessel models. Lab Chip 2015;15(22):4242–55. [PubMed: 26364747]

[57]. Allende ML, Bektas M, Lee BG, Bonifacino E, Kang J, Tuymetova G, Chen W, Saba JD, Proia RL, Sphingosine-1-phosphate lyase deficiency produces a pro-inflammatory response while impairing neutrophil trafficking. J Biol Chem 2011;286(9):7348–58. [PubMed: 21173151]

[58]. Kunkel GT, Maceyka M, Milstien S, Spiegel S, Targeting the sphingosine-1-phosphate axis in cancer, inflammation and beyond. Nat Rev Drug Discov 2013;12(9):688–702. [PubMed: 23954895]

[59]. Xu M, Waters CL, Hu C, Wysolmerski RB, Vincent PA, Minnear FL. Sphingosine 1-phosphate rapidly increases endothelial barrier function independently of VE–cadherin but requires cell spreading and Rho kinase. Am J Physiol Cell Physiol 2007;293(4):C1309–18. [PubMed: 17670896]

[60]. Gaengel K, Niaudet C, Hagikura K, Lavina B, Muhl L, Hofmann JJ, Ebarasi L, Nystrom S, Rymo S, Chen LL, Pang MF, Jin Y, Raschperger E, Roswall P, Schulte D, Benedito R, Larsson J, Hellstrom M, Fuxe J, Uhlen P, Adams R, Jakobsson L, Majumdar A, Vestweber D, Uv A, Betsholtz C, The sphingosine-1-phosphate receptor S1PR1 restricts sprouting angiogenesis by regulating the interplay between VE-cadherin and VEGFR2. Dev Cell 2012;23(3):587–99. [PubMed: 22975327]

[61]. Engelbrecht E, Levesque MV, He L, Vanlandewijck M, Nitzsche A, Niazi H, Kuo A, Singh SA, Aikawa M, Holton K. Sphingosine 1-phosphate-regulated transcriptomes in heterogenous arterial and lymphatic endothelium of the aorta. Elife 2020(9):e52690. [PubMed: 32091396]

[62]. Galie PA, Nguyen DH, Choi CK, Cohen DM, Janmey PA, Chen CS. Fluid shear stress threshold regulates angiogenic sprouting. Proc Natl Acad Sci U S A 2014;111(22):7968–73. [PubMed: 24843171]

[63]. Kang H, Bayless KJ, Kaunas R. Fluid shear stress modulates endothelial cell invasion into three-dimensional collagen matrices. Am J Physiol Heart Circ Physiol 2008;295(5):H2087–97. [PubMed: 18805898]

[64]. Kimura T, Tomura H, Mogi C, Kuwabara A, Damirin A, Ishizuka T, Sekiguchi A, Ishiwara M, Im DS, Sato K, Murakami M, Okajima F. Role of scavenger receptor class B type I and sphingosine 1-phosphate receptors in high density lipoprotein-induced inhibition of adhesion molecule expression in endothelial cells. J Biol Chem 2006;281(49):37457–67. [PubMed: 17046831]

[65]. Yanagida K, Hla T. Vascular and Immunobiology of the Circulatory Sphingosine 1-Phosphate Gradient. Annu Rev Physiol 2017;79:67–91. [PubMed: 27813829]

[66]. Camerer E, Regard JB, Cornelissen I, Srinivasan Y, Duong DN, Palmer D, Pham TH, Wong JS, Pappu R, Coughlin SR. Sphingosine-1-phosphate in the plasma compartment regulates basal and inflammation-induced vascular leak in mice. J. Clin. Invest. 2009;119(7):1871–9. [PubMed: 19603543]

[67]. Blaho VA, Hla T. Regulation of mammalian physiology, development, and disease by the sphingosine 1-phosphate and lysophosphatidic acid receptors. Chem Rev 2011;111(10):6299–320. [PubMed: 21939239]

[68]. Cartier A, Leigh T, Liu CH, Hla T. Endothelial sphingosine 1-phosphate receptors promote vascular normalization and antitumor therapy. Proc Natl Acad Sci 2020;117(6):3157–66. [PubMed: 31988136]

[69]. Ishii I, Ye X, Friedman B, Kawamura S, Contos JJ, Kingsbury MA, Yang AH, Zhang G, Brown JH, Chun J. Marked perinatal lethality and cellular signaling deficits in mice null for the two sphingosine 1-phosphate (S1P) receptors, S1P2/LPB2/EDG-5 and S1P3/LPB3/EDG-3. J Biol Chem 2002;277(28):25152–9. [PubMed: 12006579]

[70]. Nofer J-R, Van Der Giet M, Tölle M, Wolinska I, von Wnuck Lipinski K, Baba HA, Tietge UJ, Gödecke A, Ishii I, Kleuser B. HDL induces NO-dependent vasorelaxation via the lysophospholipid receptor S1P 3. J. Clin. Invest 2004;113(4):569–81. [PubMed: 14966566]

[71]. Jain RK. Normalization of tumor vasculature: an emerging concept in antiangiogenic therapy. ScienceScience 2005;307(5706):58–62.

[72]. Kamoun WS, Chae SS, Lacorre DA, Tyrrell JA, Mitre M, Gillissen MA, Fukumura D, Jain RK, Munn LL. Simultaneous measurement of RBC velocity, flux, hematocrit and shear rate in vascular networks. Nat Methods 2010;7(8):655–60. [PubMed: 20581828]

[73]. Yuan F, Salehi HA, Boucher Y, Vasthare US, Tuma RF, Jain RK. Vascular permeability and microcirculation of gliomas and mammary carcinomas transplanted in rat and mouse cranial windows. Cancer Res 1994;54(17):4564–8. [PubMed: 8062241]

[74]. Kunkel GT, Maceyka M, Milstien S, Spiegel S. Targeting the sphingosine-1-phosphate axis in cancer, inflammation and beyond. Nat Rev Drug Discovery 2013;12(9):688–702. [PubMed: 23954895]

[75]. Vickerman V, Kamm RD, Mechanism of a flow-gated angiogenesis switch: early signaling events at cell–matrix and cell–cell junctions. Integrative Biol 2012;4(8):863–74.

[76]. Sundaram PM, Rangharajan KK, Akbari E, Hadick TJ, Song JW, Prakash S. Direct current electric field regulates endothelial permeability under physiologically relevant fluid forces in a microfluidic vessel bifurcation model. Lab Chip 2021.

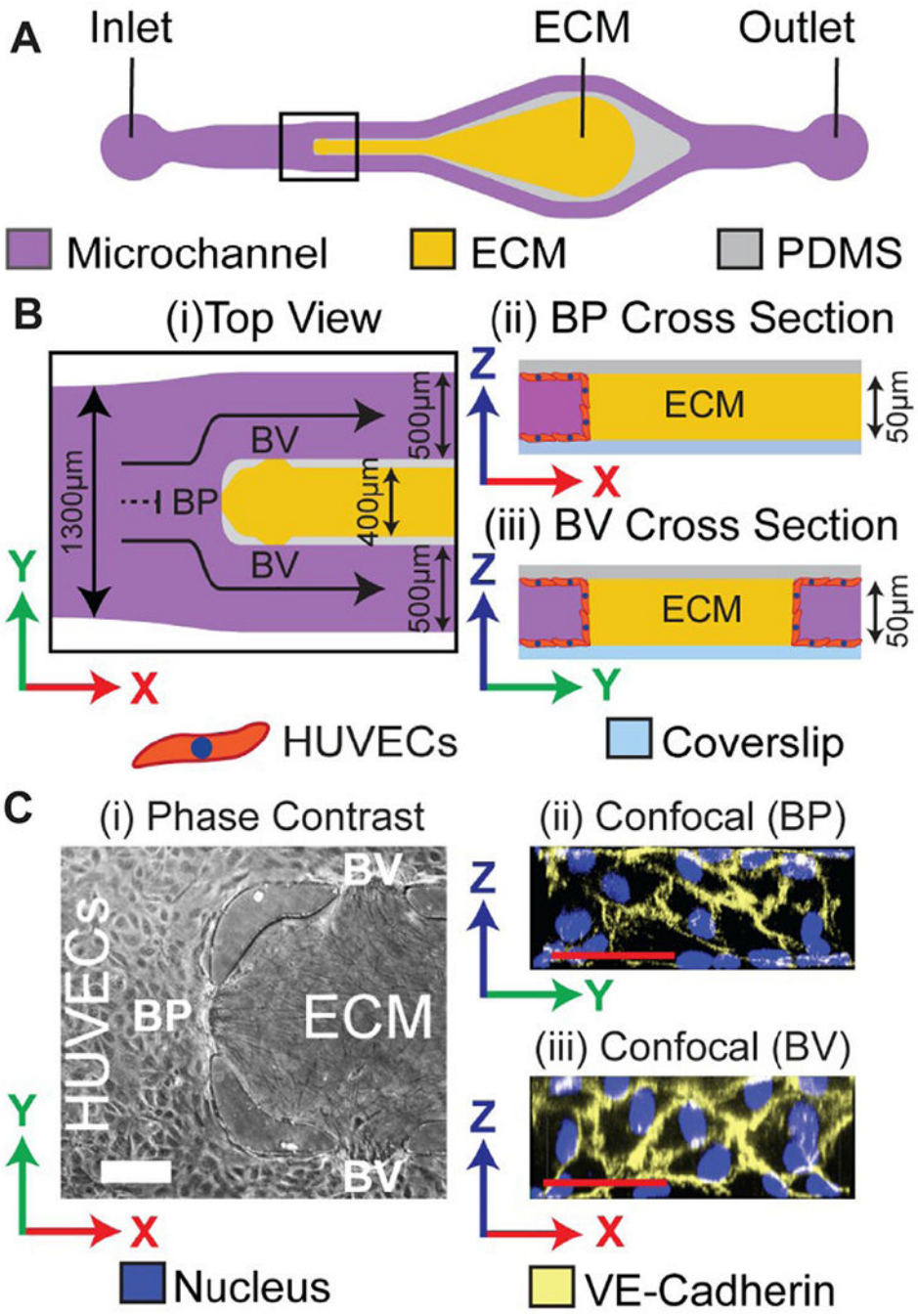

Fig. 1.

Biomimetic microfluidic model of vessel bifurcation for studying S1P-dependent L_p. (A) The device top-view schematic depicting the inlet channel bifurcating into two smaller channels around a central extracellular matrix (ECM) compartment. (B) The zoomed-in view of the bifurcation region (denoted by the black box in A). (i) Top view schematic depicts the laminar inflow stagnating on the base of the bifurcation point (BP) that results in application of bifurcated fluid flow (BFF, black dash line). Downstream of the BP, flow continues into two regions that are under laminar shear stress (LSS, black solid lines) in the

branched vessels (BV). Moreover, the apertures included in the PDMS barrier that separates the central ECM compartment from the endothelial channels allow for the formation of the endothelial monolayer at: (ii) the BP, and (iii) in each BV at the fluid-ECM interface. (C) Representative (i) phase contrast and (ii) confocal immunofluorescence images of the BP fully seeded with a confluent monolayer of HUVECs that have formed well-defined adherens junction structures. White scale bar is 100 μm. Red scale bars are 50 μm.

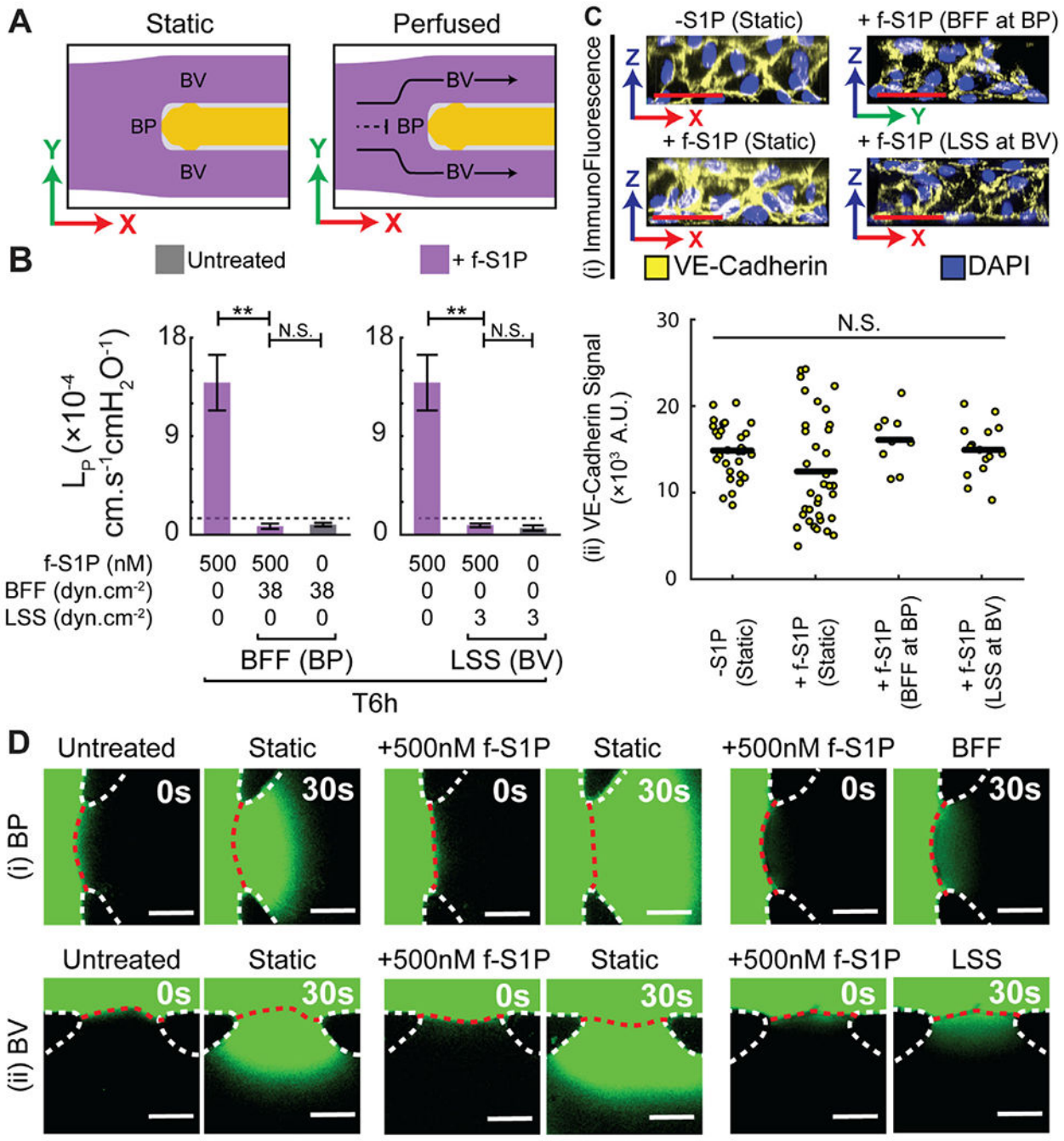

Fig. 2.

Application of BFF and LSS results in significant attenuation of increase in L_P induced by f-S1P. (A) Schematic of the experimental conditions to test the effect of BFF (black dash line) and LSS (black solid line) on S1P-dependent L_P compared to static condition. (B) Quantitative response of HUVEC L_P to treatment with f-S1P under static condition compared to treatment withf-S1P co-applied with BFF or LSS, and treatment with BFF or LSS in the absence of f-S1P. (C) Representative confocal images along with quantitative assessment of VE-cadherin expression under each experimental test condition. Blue:

HUVEC Nuclei, Yellow: VE-cadherin. (D) Representative epi-fluorescence images of FITC-Dextran extravasation rate to measure L_P at BP and BV after treatment under each experimental condition. Scale bars are 50 μm. **: $p < 0.01$, ***: $p < 0.001$.

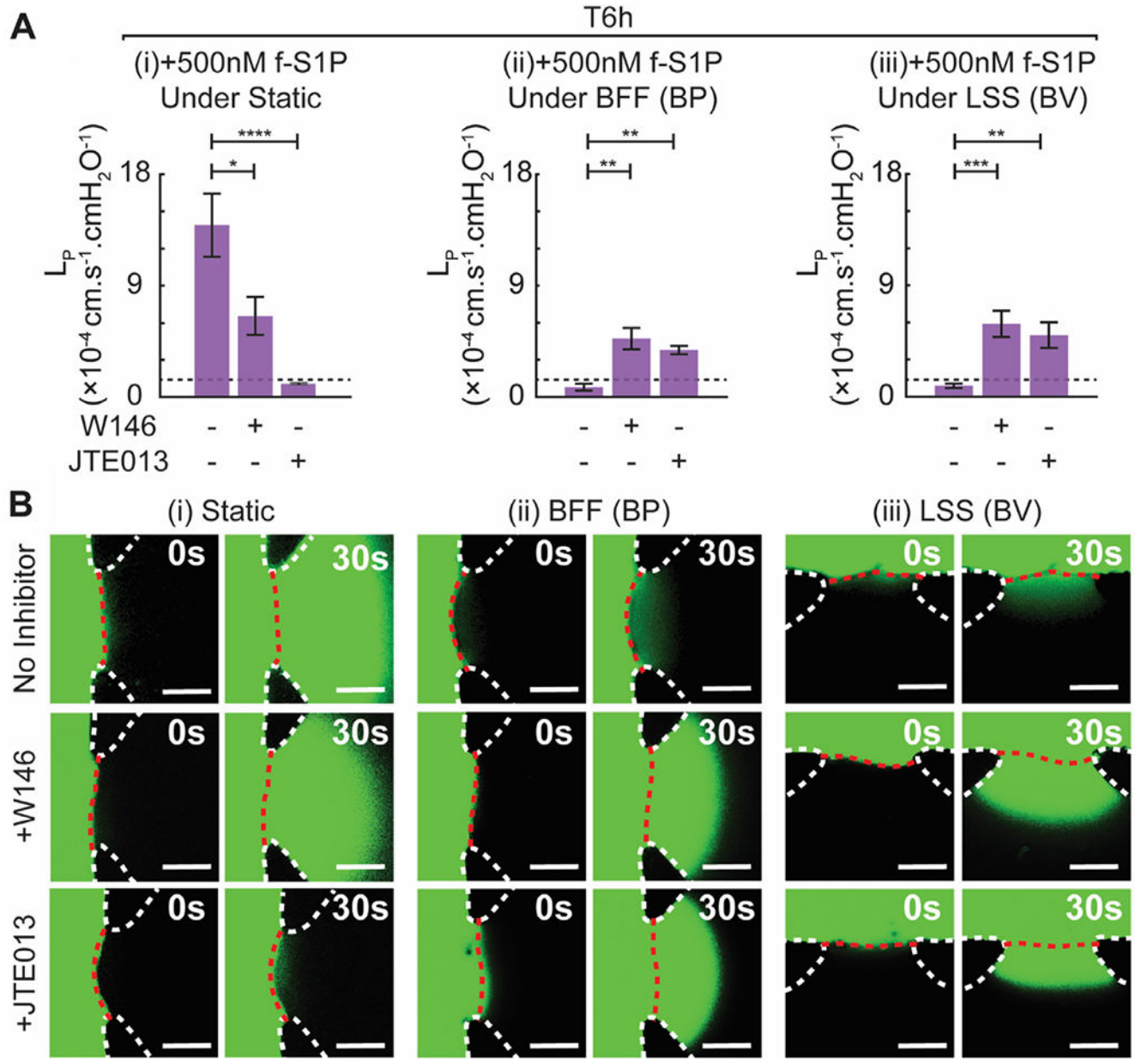

Fig. 3.

Application of BFF and LSS cause significant increase in L_P when S1PR1 or S1PR2 signaling is inhibited. (A) Quantitative bar-graph plot of HUVEC L_P in response to selective blocking of S1PR1 or S1PR2 signaling followed by treatment with 500 nM S1P for 6 h under (i) static, (ii) when co-applied alongside BFF and (iii) when co-applied alongside LSS. Black dash line denotes the baseline L_P for the static untreated condition. (B) Representative epi-fluorescence images of FITC-Dextran extravasation rate to measure L_P at BP and BV following treatment under each experimental condition. Scale bars are 50 μm. *: $p < 0.05$, **: $p < 0.01$, ***: $p < 0.001$, ****: $p < 0.0001$.

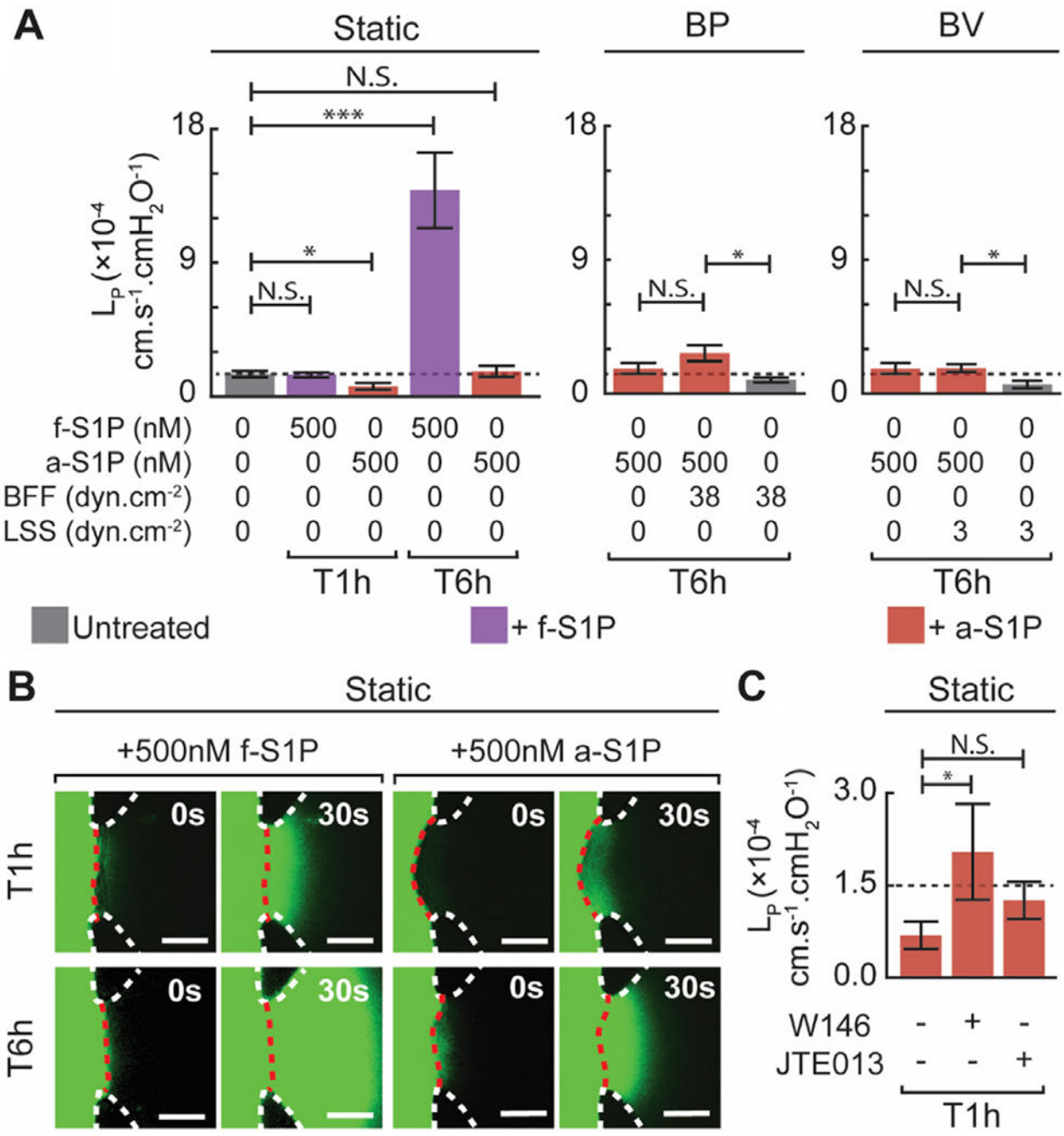

Fig. 4.

Effect of albumin associated S1P (a-S1P) on L_P. (A) Quantitative report on the time-dependent effect of a-S1P on L_P under static condition, 38 dyn•cm^{-2} BFF at BP and 3 dyn•cm $^{-1}$ LSS at BV. Black dash line denotes the baseline L_P for the static untreated condition. (B) Representative epifluorescence images of the BP aperture depicting the extravasation rate of FITC-Dextran during L_P measurement following treatment with f-S1P versus a-S1P. (C) Role of S1PR1 and S1PR2 signaling in mediating temporal stabilization of HUVEC monolayer by a-S1P under static condition. Blocking S1PR1 signaling with W146

significantly inhibited the observed stabilizing effect of treatment with a-S1P for 1 hour. In contrast, blocking S1PR2 signaling with JTE013 followed by treatment with a-S1P for 1 hour did not cause a significant change in L_P compared to the case treated with a-S1P for 1 hour without any S1P receptor inhibition. *: $p < 0.05$, ***: $p < 0.001$.